

Review of the recent x-ray and neutron powder diffraction studies on lead zirconate titanate

J. Frantti

Laboratory of Physics, Helsinki University of Technology, P.O. Box 4100, FIN-02015 HUT, Finland*

(Dated: September 25, 2018)

The issues related to the structure refinement of $\text{Pb}(\text{Zr}_x\text{Ti}_{1-x})\text{O}_3$ (PZT) solid solutions are discussed. Particular attention is paid on the modelling of the co-existing phases in the vicinity of the morphotropic phase boundary (MPB), where local symmetry is often significantly lower than the average symmetry. According to recent studies, two-phase co-existence in the vicinity of the MPB is a thermodynamical necessity. Significantly different structural models for PZT with x in the vicinity of the MPB have recently been published. Structural models, based on x-ray, neutron and electron diffraction studies, are reviewed and two essentially different approaches were identified: (i) a method where space group symmetry was decreased until the features due to the local distortions were 'modelled' and (ii) a method where the highest space group symmetry compatible with the powder diffraction data was used together with a model for a local disorder. Related to the method (ii), the essential features of a model taking the hkl -dependent line broadening into account are summarized. The importance of the cationic disorder is demonstrated by computing the variation in Madelung energies due to the variation in structural parameters for PZT using experimental data. The underlying theme is to consider how local regions, with symmetry lower than the average symmetry, should be modelled. Method (i) often introduces unjustified structural parameters and should be avoided. By studying the temperature and composition dependence of the structural parameters, including line shape parameters and phase fractions in the case of the two phase samples, one can further test the proposed models. The significance of the local structure for electrical properties (switchable polarization and electrical conductivity) is discussed by considering the local Pb ion displacements and their dependence on the neighbouring B -cation configuration. The connection between the structure and piezoelectric properties, with emphasis on the co-existence of the rhombohedral and monoclinic phases, is discussed in light of the recent first-principles computational studies. Also problems connected to sample preparation and data collection are pointed out.

PACS numbers: 77.84.Dy 61.12.Ld 61.50.Ah 81.30.Dz

I. INTRODUCTION

Lead zirconate titanate [$\text{Pb}(\text{Zr}_x\text{Ti}_{1-x})\text{O}_3$, (PZT)] solid solutions are among the most widely used ferroelectric ceramics. The importance of PZT ceramics with morphotropic phase boundary (MPB) compositions is due to the exceptionally good piezoelectric properties they exhibit¹, which in turn has motivated numerous studies seeking physical mechanisms responsible for this extraordinary behaviour (for a summary of the various studies see ref. 2). Crystal structure studies and the changes in atomic positions versus composition, temperature, pressure or electric field have a central role for the understanding of these materials: nuclei positions, together with the electron density, determine the electric polarization vector on which the numerous applications are based on. It is essential to understand how the polarization vector changes as a function of electric field, composition, temperature or pressure. Qualitatively, the average structural tendencies versus composition, temperature or pressure of ionic compounds, such as PZT, can be understood by considering the Madelung energies which decreases with decreasing crystal volume until the shortrange interactions balance the crystal volume to its equilibrium value. For ionic crystals the contribution of Madelung energy to the total energy is dominant

and implies that crystal volume tends to be minimized. By tilting the oxygen octahedra the crystal can partially compensate for the effect of a larger average B -cation (Zr and Ti) size which increases with increasing Zr content x . This is seen from the behaviour of Zr rich samples: once crystal adopts $R3c$ symmetry, instead of $R3m$ symmetry, the volume per primitive cell is smaller. This is consistent with the notion that in the case it would cost a lot of energy to contract the oxygen octahedra (due to the shortrange interactions which cause the mere compression of octahedra to be energetically unfavourable) overall energy gain can still be obtained by tilting the oxygen octahedra. This can neatly be expressed through the equation $V_A/V_B \approx 6 \cos^2 \langle \omega \rangle - 1$, where V_A and V_B are the polyhedral volumes for A and B cations and $\langle \omega \rangle$ is the mean octahedral tilt angle³. This expression means that when there is no chance for oxygen octahedra to decrease its volume the crystal can still be compressed by decreasing the volume of the cuboctahedra surrounding the A cation. Typically the changes in octahedral tilts occur consistently versus composition⁴ or temperature⁵ and thus particular care is necessary before anomalous octahedral tilt systems are considered. Secondly, in the case of PZT (and other Pb containing perovskite ferroelectrics) the crystals suffer from numerous defects. These defects do have a significant role for

ferroelectricity. An example is provided by the Pb ions which are significantly displaced from their ideal sites and which respond to the external electric field or pressure by adjusting their position with a corresponding changes in polarization vector^{6,7}. As was discussed in ref. 8, it is not clear if Pb displacements are dominantly dynamic or static. Static displacements have commonly been modelled by displacing Pb ions towards $\langle 110 \rangle$ directions and using isotropic atomic displacement parameters (ADP), whereas the dynamic contribution was modelled by anisotropic ADP parameters. In some cases, one can try to distinguish the static and dynamic contributions by collecting structural data as a function of temperature⁹. In PZT and PbTiO₃ crystals the contribution of anharmonic terms to the potential is significant, as was demonstrated by Raman scattering studies in the case of PbTiO₃^{10,11} and PZT¹², and obscures the separation of static and dynamic contributions. Similar situation occurs in many Pb and Bi containing perovskites and is often believed to be an important factor allowing a co-existence of ferromagnetic and ferroelectric ordering in multiferroic perovskites¹³. Related consideration holds for Zr and Ti, whose positions are disordered in two ways: (i) the probability that the B-cation site is occupied by Zr (Ti) is x ($1 - x$) and (ii) the fractional coordinates of Zr and Ti are different. The confirmation of the assumption (i) is not straightforward, but various powder diffraction and Raman scattering studies show that it is a good approximation for most cases. By high resolution powder diffraction instruments it is possible to study these peculiar features by extracting information from the line shapes, in addition to the determination of the average structure. However, it became apparent that a rather complex lineshape is necessary for the modelling of the diffraction peak profiles, for examples see refs. 14 and 15. The structure of the PZT ceramics with composition in the vicinity of the MPB are notoriously tricky to model. In addition to the aforementioned structural distortions there are two other reasons obscuring the modelling work: (i) in practice, no single phase samples are obtained, instead one observes two perovskite phases and (ii) diffraction peak profiles are rather complex. Both factors are connected to the fact that this 'boundary' separates tetragonal and rhombohedral phases which do not possess a group-subgroup relationship. The experimental observation that monoclinic Cm phase separates tetragonal (space group $P4mm$) and rhombohedral (at room temperature space group is $R3m$) phases clarified the situation: Cm is a common subgroup of $P4mm$ and $R3m$ phases^{6,7}. Correspondingly, instead of morphotropic phase boundary one occasionally refers to morphotropic phase^{6,7}. Thus, it is not a surprise that the structural disorder is particularly pronounced in the vicinity of MPB. This is also partially due to fact that typically the structure and composition of the grain boundaries and bulk are different. This is revealed from the Bragg reflection line shapes, which are almost 'Gaussian' like at room temperature^{7,16} in the

case of the less abundant phase. Even though it is still an open question whether Cm is stable phase in PZT system it provides an explanation to the peak value of piezoelectric constant via the polarization rotation theory: first-principles computations demonstrated that the polarization rotation provides the lowest free energy path along which there is a large coupling between the polarization and the electric field¹⁷, consistently with the experimentally observed large electromechanical response. Thermodynamical consideration of the polarization rotation within monoclinic phase and its impact on piezoelectric properties is given in ref. 8. This study addresses the question if it is necessary to invoke the monoclinic phase to explain the observed piezoelectric properties.

Recently, a model which used two monoclinic phases (space group symmetries Cc and Cm) was claimed to be the correct low-temperature structure of PZT with $x \approx 0.52$ ¹⁸, see also note 19 and refs. 20 and 21. This report stated that $R3c$ symmetry is not a correct choice for PZT with $x \approx 0.52$ ¹⁸. The fact that superlattice reflections allow the distinction of $R3c$ and Cc symmetries in favour of the former was overlooked in this study. Nevertheless, Cc symmetry predicts reflections well isolated from those of the $R3c$ symmetry. To summarize the models proposed in refs. 18 and 20, we note that the phase which traditionally has been assigned to the rhombohedral symmetry¹, was assigned to Cm symmetry and space group symmetry $P4mm$ (at room temperature) or Cc (at low temperature) was assigned to the phase which was modelled by Cm symmetry in refs. 5,6 and 7. Thus, significant changes to the well known PZT phase diagram¹ were proposed. To understand the problems related to such a model (abbreviated as $Cc + Cm$) and the reason why the use of space group Cc was previously rejected⁵ it is necessary to summarize the crucial role of the local disorder resulting in hkl -dependent line broadening²². Erroneous space group symmetry assignments likely result in once this line broadening is compensated for by reducing the space group symmetry²³. The hkl -dependent line broadening is an *inherent* property of PZT powders due to the local distortions, and is already seen in tetragonal Ti rich compositions and even at high temperature cubic phase²⁴. Namely, the Bragg reflection widths were anisotropic already at the cubic phase, although the linewidths were an order of magnitude smaller than in the case of the low-temperature phases. It is well known that broad peaks are observed in Raman spectra collected at high temperature cubic phase, even though no first order Raman scattering is allowed for the ideal symmetry. For example, see ref. 25, where the modes appearing in cubic phase were assigned to the first order scattering, activated by the local disorder, by studying the temperature dependence of the intensities. The same behaviour was observed in a closely related Pb(Hf _{x} Ti _{$1-x$})O₃ (PHT) system with $0.10 \leq x \leq 0.40$, where the peak widths of the $00l$ reflections were *twice* as large as the widths of $h00$ reflections²⁶. It must be emphasized that no signs of symmetry lowering from the

$P4mm$ symmetry was observed in this high-resolution neutron powder diffraction study. In contrast, light scattering experiments revealed that both in the case of tetragonal PZT and PHT samples deviations from the average symmetry were observed^{27,28,29}. Namely, the number of Raman active modes was larger than the symmetry found by diffraction techniques would allow. Once the diffraction patterns were examined it became apparent that there was no justification to use lower space group symmetry. A model based on lower space group symmetry would simply result in physically meaningless structural parameters. In this case, the essential point was that even if one insist to invoke lower space group symmetry in order to explain the observed Raman spectra the changes in bond lengths should be so large that also high resolution neutron powder diffraction patterns should reveal it. Although one can decrease the average symmetry to decrease the residuals, a more realistic model is obtained by assuming that (i) the *average symmetry* over a length scale of a few hundred nanometers is $P4mm$, and (ii) deviations from this symmetry occur in a local scale (of a few unit cells). The essential point here is that these deviations are not periodical, at least not in a scale probed by x-ray or neutron diffraction. However, ion displacements (particularly those of Pb ions) are likely correlated in a scale of a few unit cells². It is also worth mentioning that usually there are several line broadening mechanisms. Especially powders consisted of fine crystallites, typically obtained through wet chemical methods allowing a preparation of perovskite phase at rather moderate temperatures, show large broadening due to the small crystallite size, in addition to the anisotropic line broadening³⁰. Williamson-Hall plot was constructed to separate crystallite and anisotropic strain broadening effects³⁰ in tetragonal PZT. This study revealed that the lattice strain is greater along the [001] directions than along the [100] directions. On the other hand, samples prepared through solid state reaction often have an order of magnitude larger crystallite size. In the case of PZT with compositions in the vicinity of the MPB the line widths are strongly increasing with decreasing temperature²⁴, demonstrating that the crystallite size and shape alone cannot account for the observed line broadening behaviour. Similar, although weaker, phenomenon occurs in the case of tetragonal PZT and PHT samples.

Transmission electron microscopy (TEM) and electron diffraction (ED) studies revealed extra reflections in rhombohedral PZTs³¹. The origin of these reflections was more recently studied by TEM and ED together with neutron powder diffraction (NPD) techniques³². In this study superlattice reflections of the type R_1 , R_2 , M_1 and M_2 (see Table I) were observed, consistently with ref. 31. Among these reflections only R_2 is consistent with $R3c$ symmetry³². We summarize the observations and interpretations given in ref. 32 as follows: (i) M -type reflections were accompanied by satellites, (ii) different areas in the same grain resulted in changes in the relative

TABLE I: . Classification of superlattice reflections commonly found in the rhombohedral phases of PZT by TEM/ED studies. Tilts refer to Glazer notation³³. Table is adapted from ref. 32.

Type	Reflection	Conditions	Tilt
R_1	$\frac{1}{2}\{hkl\}_p$	$h = k = l$	None
R_2	$\frac{1}{2}\{hkl\}_p$	$h \neq k \neq l$	a^-
M_1	$\frac{1}{2}\{0kl\}_p$	$k = l$	None
M_2	$\frac{1}{2}\{0kl\}_p$	$k \neq l$	a^+

intensities of the superlattice reflections so that in some cases the extra spots completely disappeared, (iii) by collecting data on samples prepared from single crystals and ceramics it was found that the satellites around M points are characteristic feature of only ceramics, (iv) by studying the temperature dependence of the extra reflections they could be assigned to the ferroelectric state (no extra reflections were observed at cubic phase), (v) octahedral tilts and distortions alone are insufficient to explain R_1 and M superlattice reflections *with the intensities observed* (it was demonstrated that very weak superlattice reflections could be obtained using unrealistically large oxygen octahedra tilts and distortions), and (vi) NPD experiments revealed *only* R_2 reflections, consistently with an average $R3c$ symmetry. To explain these observations models based on locally ordered regions presenting antiparallel cation displacements were proposed (see also ref. 4 where structural models based on NPD experiments are given) and compared with experiments. Finite size effect was proposed as an underlying reason for the phenomena observed by TEM and ED techniques. This is an important point since it suggests that *these puzzling phenomena, observed by TEM and ED techniques, do not occur in the case of bulk ceramics*. However, the tendency of Pb ions to form four short bonds with oxygen is a feature observed through NPD studies⁴. This tendency is also seen from the models constructed to explain the observed ED patterns³². It is also worth to note that similar conclusions were obtained through Monte Carlo simulations: M -like superlattice reflections are not present in pure bulk crystals but might be locally induced by surfaces over some range of temperature³⁴.

After a reasonable model for local distortions or locally ordered regions is identified a selection of an appropriate instrument for the (preferably neutron) powder diffraction experiments to further test the structural models is essential. For example, the Cm phase was identified by studying the peak split of the pseudo-cubic 110 reflections^{6,7} through high resolution synchrotron experiments. This peak split was beyond the resolution of the instrument used in ref. 18 and there is no way to recover the lost information. Thus, new refinements do not compensate for the problems connected to the low-resolution data collected with insufficient counting time. The role of the spatial composition variation (which in practice can-

not be eliminated) in the vicinity of the phase boundary is an old and still a valid explanation for the two phase 'co-existences' and also largely explains the hkl -dependent line broadening. A qualitative model which was constructed by studying changes in structures and their mutual phase fractions versus temperature and x was proposed in refs. 5 and 24. These aspects are reviewed below. In section II the variance in Madelung energies, corresponding to the variance in experimentally determined structural parameters, is given for PZT. The idea of this consideration is not to give a qualitative treatment for the total energy of disordered PZT system but to demonstrate the crucial role of disorder by showing that rather small variations in structural parameters correspond to large variation in Madelung energy. Various Pb-ion displacement configurations observed in different phases of PZTs are addressed in section III. This section reviews the physical origin of Pb-ion displacement and its effect on modelling and electrical properties. In section IV we discuss the role of the spatial composition variation on the PZTs with x in the vicinity of the MPB, as it is closely connected to the two phase co-existence. The main goal of the section IV is to provide an explanation for the different type of domains by taking into account the recent thermodynamical considerations and to show that these ideas are consistent with numerous experimental observations. Anisotropic line broadening is discussed in section V. Section VI reviews different two-phase models proposed for PZT in the vicinity of MPB. Section VIII summarizes the results obtained through bond-valence computations and recent computational studies.

II. MADELUNG ENERGIES FOR PZT SYSTEM

The Madelung energy was computed by applying the Ewald method^{35,36}. The Madelung energy is given by the equation $E_M = \sum_{kk'} z_k z_{k'} \alpha_{kk'} / (\epsilon_0 r)$, where the summation runs over all ions k and k' (with charges z_k and $z_{k'}$, respectively) in a primitive cell (assumed to be charge neutral) and ϵ_0 is the permittivity of free space. Charges were assumed to be integer multiples of the electric charge e . Following refs. 35 and 36 the coefficients $\alpha_{kk'}$ are written as

$$\begin{aligned} \alpha_{kk'} = & \frac{1}{2} c \sum_{l'}' H(c|\mathbf{x}_{l'k'} - \mathbf{x}_{0k}|/r) - \delta_{kk'} c / \sqrt{\pi} + \\ & + \pi / (2c^2 s) \sum_{hkl}' G(\pi^2 |\mathbf{b}(hkl)|^2 r^2 / c^2) \exp[2\pi i \mathbf{b}(hkl) \cdot \\ & (\mathbf{x}_{0k'} - \mathbf{x}_{0k}) r^2 / c^2], \end{aligned} \quad (1)$$

where $H(x) = (1/x) \operatorname{erfc}(x)$ (erfc is the complementary error function), $G(x) = (1/x) \exp(x)$, $\delta_{kk'}$ is the Kronecker delta function, \mathbf{x}_{lk} is the position of the ion k at the primitive cell l , $\mathbf{b}(hkl)$ is a primitive reciprocal lattice vector (indexed by integers h, k, l and defined without the prefactor 2π) and v is the volume of the primitive cell, $v = sr^3$. Primes above the summation signs indicate

that in the first (real space) sum the term $\mathbf{x}_{l'k'} = \mathbf{x}_{0k}$ is omitted, and in the case of the second (reciprocal lattice) sum the term $\mathbf{b}(hkl) = 0$ is omitted. Number c controls the convergence of the two sums, and was selected so that both the real and reciprocal lattice sums were of the same order of magnitude. The coefficients $\alpha_{kk'}$ do not depend on the value of c ($d\alpha_{kk'}/dc$ vanishes for all c). However, by selecting too small or too large value for c results in a situation where either the reciprocal or real lattice sum vanishes (within the numerical accuracy of the computational routines), leading to erroneous values for $\alpha_{kk'}$. We fixed c at π .

Crystal structure data for PZT ceramics were adapted from refs. 5, 24 and 37 (high pressure data). To simplify the computational task, we assumed that the fractional z coordinates for both B cations are the same (though they differed in the case of the tetragonal perovskites, see Table VI in ref. 5). Thus, for this case the z coordinate values for the B cations were computed using an equation $z(B) = x \times z(\text{Zr}) + (1 - x) \times z(\text{Ti})$ (this approximation was used for $x = 0.20, 0.30$ and 0.40 data). Similar approximation was also done for the fractional x coordinates of the $x = 0.52$ PZT sample. In addition, we assumed that Pb ions were fixed at origin. During the Rietveld refinement they were allowed to shift towards the $\langle 110 \rangle$ directions. Ionic charges were fixed at their nominal values (+2 for Pb, +4 for the B cations, and -2 for O). An error estimation for the Madelung energy was carried out using the standard deviation values of the structural parameters. The error estimates of the structural parameters were assumed to be independent. It is worth to note that the error estimates are specific to the structural model. For instance, for the cubic symmetry there is only one structural parameter, the a axis value, while there are 11 structural parameters for Cm phase. This resulted in significantly larger error estimates for Cm phase.

Figure 1 shows the room temperature Madelung energies for PZT ceramics versus x and, for the $x = 0.54$ sample, versus temperature. The Madelung energy increases almost linearly with increasing x (when $x \leq 0.50$), as is seen from Fig. 1 (a). This is related to the fact that the average bond lengths increase with increasing x . However, octahedral tilt ($R3c$ phase) and collective Pb ion shifts (Cm phase) correspond to a small energy gain. Both are features which were neglected in the present treatment of tetragonal PZT. It was interesting to note that, in the vicinity of the MPB, $P4mm$ ($x = 0.50$), Cm and $R3c$ phases ($x = 0.52$) had almost the same Madelung energies: Cm phase had the lowest energy, while the energy of $R3c$ phase was almost the same, and approached the energy of Cm phase with increasing x (Fig. 1 (a)). This is consistent with the observed phase transition sequence against x . As the difference between Madelung energies of Cm and $R3c$ phases in the vicinity of MPB is small, it is not a surprise that a preparation of single phase samples within this composition range is very difficult. Also the evolution of Madelung

energies versus temperature indicates that the difference between the Madelung energies of Cm and $R3c$ phases is small up to room temperature, see Fig. 1 (b). The Madelung energy of $R3c$ phase at 583 K should be treated with caution, since $R3c$ phase fraction at this temperature was very small (correspondingly, the structural data were not very accurate). It is clear from Fig. 1 (b) that the Madelung energy solely does not explain the observed temperature dependent phase fractions seen in PZT with $x = 0.54$ sample²⁴: Cm and $R3c$ phases had almost the same Madelung energies, and it was only at around 583 K that the difference became significant. Although the given treatment is rather crude, it points out that both local cation shifts and octahedral tilts are mechanisms to be considered. The first one is significant through the whole composition range whereas the latter cannot be neglected at high Zr concentrations.

III. LOCAL DISORDER: PB ION DISPLACEMENTS VERSUS x

The physical origin of the Pb-ion displacement in a local scale is often connected to the $6s^2$ lone electron pair (L) which makes displaced position energetically more favourable (actually one must also consider the $6p$ states, as discussed below). An insight to the important role of L can be obtained by considering the formation of $PbTiO_3$ by alloying the litharge phase of PbO and TiO_2 , as shown in ref. 38. In the case of $Pb_{1-x}(TiO)_xO$ solid solution a TiO_2 group is substituted for a $PbOL$ group and the extra oxygen fills the volume of L . Thus, due to L Pb prefers to form four short Pb-O bonds in a pyramidal configuration, a tendency which is also seen in different phases of PZT: to fulfill this criteria Pb ions are displaced from their average positions (although the resulting PbO_4 pyramid is no more symmetric). As was discussed in ref. 4, this occurs in the orthorhombic, tetragonal and rhombohedral phases of PZT. In other words this means that Pb ion is not located at the centre of the oxygen cuboctahedra, not even in the cubic phase. In ref. 4 local structures capable of producing the extra reflections of the type $\{\frac{1}{2}, \frac{1}{2}, 0\}_P$ (Fig. 7) and $\{\frac{1}{2}, \frac{1}{2}, \frac{1}{2}\}_P$ (Fig. 8) seen in TEM and ED studies *at approximately the correct intensities* are given. This picture gives a qualitative idea concerning the Pb ion displacements with respect to its nearest neighbours. Correspondingly, one must consider the whole oxygen and B-cation network in order to determine the overall Pb-displacement pattern. Table II summarizes the average structures of PZT system with typical structural parameters. Fig. 2 shows the commonly assumed Pb-ion displacements for tetragonal PZT, PZT with x in the vicinity of the MPB (Cm symmetry) and $PbZrO_3$. Fig. 2 demonstrates that there are numerous ways to displace Pb ions to form short Pb-O bonds: in $PbZrO_3$ Pb ions are displaced in such a way that an antiferroelectric ordering results in in ab plane³⁹. Rough but illustrative picture for this can be obtained by considering the tolerance fac-

tor $t = (R_A + R_O)/(\sqrt{2}(R_B + R_O))$ where R_A , R_B and R_O are the ionic radii for the A- and B-cations and oxygen. In the case of $PbZrO_3$ $t < 1$ implying that the Pb ions are not able to fill the cuboctahedra, whereas Zr fills octahedra so tightly that it takes a larger share from the total volume by tilting the octahedra. In this sense one can 'construct' $PbZrO_3$ by (i) considering the large Zr ions, which results in a $a^-a^-c^0$ tilt corresponding to distorted oxygen octahedra and then (ii) displacing Pb ions inside the cuboctahedra in such a way that four short, essentially covalent, bonds with oxygen (constituting a PbO_4 'pyramid') are formed. Very similar situation occurs in a closely related $PbHfO_3$ which is isostructural and has the same space group symmetry as $PbZrO_3$ ⁴⁰. For clarity it must be said that the given treatment is meant to be illustrative and not to give any causality relationships (in ref. 40 the type of octahedral tilting and deformation was seen as a way to accommodate the nature of the Pb-O bonding). Now, the PbO_4 pyramids alternate in the ab plane in such a way that antiferroelectric ordering is formed. Also the Zr ions experience similar shifts, although the absolute variation in Zr-O bonds (at 100 K the shortest and largest Zr-O bonds were 2.41 and 3.105 Å) is not that large as in the case of Pb-O bonds (at 100 K the shortest and largest Zr-O bonds were 2.044 and 2.205 Å). In contrast to Pb ions Zr ions exhibit antiparallel [001] shifts³⁹. Also the behaviour of the Pb(1) and Pb(2) ions (specified in table II versus temperature was found to be different. Namely, at 100 K the Pb(1) ion shift was significantly larger than that of the Pb(2). Thus changes in Pb(1) position were larger than those of Pb(2) once the cubic phase was approached. It is interesting to note that in the case of Pb(1) three of the Pb-O bonds in PbO_4 pyramid were much shorter than the fourth one so that Pb(1) is almost threefold coordinated. In this context it is worth to mention that $Pbam$ and $R3m$ phases do not have group-subgroup relationship nor is common subgroup reported to exist between the two phases (in contrast to the case of MPB). Interestingly, there is a very narrow (with respect to temperature and x) region where $PbZrO_3$ and PZT with very small amount of Ti with $Pbam$ symmetry transforms into ferroelectric rhombohedral phase at around 500 K. However, the stability region of this phase is very sensitive to impurities⁴¹ and Pb ion positions are disordered⁴². Both phase transitions $Pbam \rightarrow R3m$ and $R3m \rightarrow Pm\bar{3}m$ are first order transitions (first necessarily by the given symmetry arguments)⁴¹. Since the Pb ion displacements from their ideal cubic sites are dominant in $PbZrO_3$ (so that the Pb ion are shifted with respect to the Zr and oxygen ions, which remain at their ideal sites) they essentially measure the sublattice polarization. Thus it is possible to simplify the structural model which in turn allows one to write down a simple free energy expansion⁴¹ for $PbZrO_3$.

In contrast, Pb-ions displacements average out in tetragonal PZT so that there is no net polarization in ab plane. This is often modelled by assuming that the four $(xx0)$ sites, equivalent in the case of $P4mm$ sym-

TABLE II: Average space group symmetries and representative values for structural parameters reported for PZT system. Note that sometimes the positions of Zr and Ti were refined independently. In the case of the rhombohedral phases the structural parameters refer to the hexagonal setting. Customarily $R3c$ symmetry has been used to describe the $R3m$ phase by setting $e = 0$ (correspondingly the c axis is halved). Thus only $R3c$ phase is specified. Lattice vectors and oxygen octahedra tilts are given in terms of pseudocubic lattice vectors. x_{Zr} refers to Zr content. Deviations from these symmetries are discussed in text.

Space group	Lattice vectors	Ion	Multiplicity and Wyckoff letter	x	y	z	Tilt	Typical values for structural parameters	T/K	x_{Zr}	Ref.
$Pm\bar{3}m$	$\mathbf{a}_c = \mathbf{a}_p$						$a^0 a^0 a^0$	$a_c = 4.080\text{\AA}$	773	0.54	24
		Pb	1a	0	0	0					
		Zr/Ti	1b	1/2	1/2	1/2					
		O	3c	1/2	1/2	0					
$P4mm$	$\mathbf{a}_t = \mathbf{a}_p$						$a^0 a^0 a^0$	$a_t = 3.978\text{\AA}, c_t = 4.149\text{\AA}$	295	0.30	5
	$\mathbf{c}_t = \mathbf{c}_p$	Pb	4d	x	y	0		$x = y = 0.015$			
		Zr/Ti	1b	1/2	1/2	z		$z_{\text{Zr}} = 0.560, z_{\text{Ti}} = 0.547$			
		O(1)	1b	1/2	1/2	z		$z_{\text{O}(1)} = 0.101$			
		O(2)	2c	1/2	0	z		$z_{\text{O}(2)} = 0.617$			
Cm	$\mathbf{a}_m = \mathbf{a}_p - \mathbf{b}_p$						$a^0 a^0 a^0$	$a_m = 5.722\text{\AA}, b_m = 5.710\text{\AA}, c_m = 4.137\text{\AA}, 20^\circ$		0.52	7
	$\mathbf{b}_m = \mathbf{a}_p + \mathbf{b}_p$	Pb	2a	0	0	0		$\beta = 90.498^\circ$			
	$\mathbf{c}_m = \mathbf{c}_p$	Zr/Ti	2a	x	0	z		$x_{\text{Zr/Ti}} = 0.477, z_{\text{Zr/Ti}} = 0.551$			
		O(1)	2a	x	0	z		$x_{\text{O}(1)} = 0.449, z_{\text{O}(1)} = 0.099$			
		O(2)	4b	x	y	z		$x_{\text{O}(2)} = 0.212, y_{\text{O}(2)} = 0.257, z_{\text{O}2} = 0.627$			
$R3c$	$\mathbf{a}_h = \mathbf{a}_p - \mathbf{b}_p$						$a^- a^- a^-$	$a_h = 5.824\text{\AA}, c_h = 14.372\text{\AA}$	295	0.80	4
	$\mathbf{b}_h = \mathbf{b}_p - \mathbf{c}_p$	Pb	6a	0	0	$s + 1/4$		$s = 0.032$			
	$\mathbf{c}_h = \mathbf{a}_p + \mathbf{b}_p + \mathbf{c}_p$	Zr/Ti	6a	0	0	t		$t_{\text{Zr}} = 0.014, t_{\text{Ti}} = 0.025$			
		O	18b	$1/6 - 2e - 2d$	$1/3 - 4d$	$1/12$		$e = 0.012, d = -0.003$			
$Pbam$	$\mathbf{a}_o = \mathbf{a}_p - \mathbf{b}_p$						$a^- a^- c^0$	$a_o = 5.884\text{\AA}, b_o = 11.787\text{\AA}, c_o = 8.231\text{\AA}$	100	1	39
	$\mathbf{b}_o = 2(\mathbf{a}_p + \mathbf{b}_p)$	Pb(1)	4g	x	y	0		$x_{\text{Pb}(1)} = 0.699, y_{\text{Pb}(1)} = 0.130$			
	$\mathbf{c}_o = 2\mathbf{c}_p$	Pb(2)	4h	x	y	1/2		$x_{\text{Pb}(2)} = 0.707, y_{\text{Pb}(2)} = 0.123$			
		Zr	8i	x	y	z		$x_{\text{Zr}} = 0.242, y_{\text{Zr}} = 0.124, z_{\text{Zr}} = 0.249$			
		O ₁	4g	x	y	0		$x_{\text{O}(1)} = 0.296, y_{\text{O}(1)} = 0.097$			
		O ₂	4h	x	y	1/2		$x_{\text{O}(2)} = 0.278, y_{\text{O}(2)} = 0.156$			
		O ₃	8i	x	y	z		$x_{\text{O}(3)} = 0.036, y_{\text{O}(3)} = 0.262, z_{\text{O}(3)} = 0.220$			
		O ₄	4f	0	1/2	z		$z_{\text{O}(4)} = 0.297$			
		O ₅	4e	0	0	z		$z_{\text{O}(5)} = 0.270$			

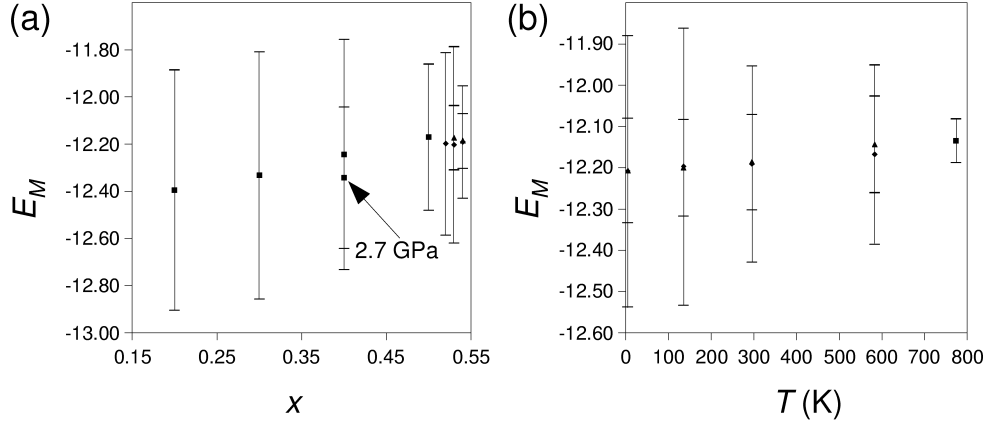


FIG. 1: The Madelung energies (in units of $\epsilon_0 \text{\AA}/e^2$) of PZT crystals per formula unit (a) versus composition x at room temperature, (b) versus temperature in the case of the $x = 0.54$ sample. E_M values correspond to $P4mm$ phase for $x \leq 0.50$ and, in the case of the $x = 0.52, 0.53$ and 0.54 samples, values for Cm (squares) and $R3c$ (triangles) phases are given. The 773 K value corresponds to $Pm\bar{3}m$ phase. For $x = 0.40$ sample, the structural data for 2.7 GPa value was adapted from ref. 37. In the case of the two phase samples, the larger error bars correspond to Cm phase, see text.

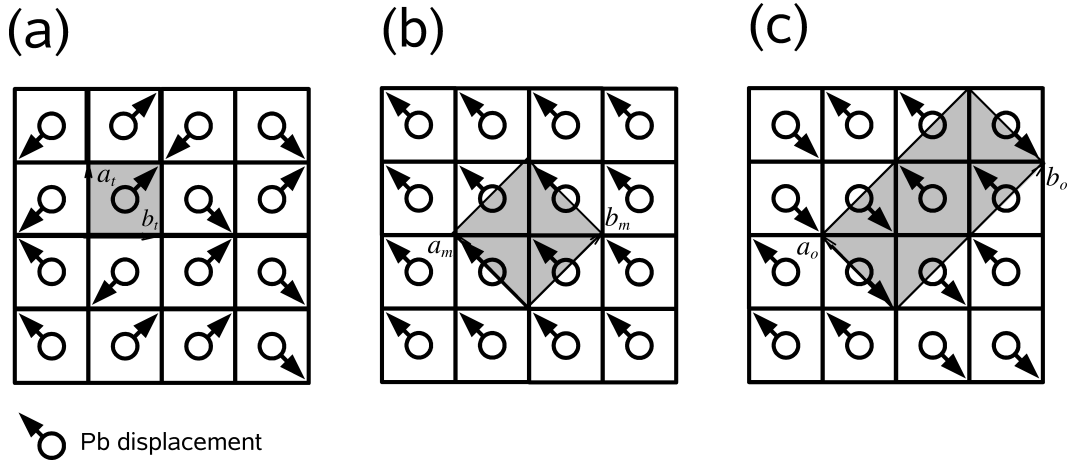


FIG. 2: Pb-ion displacements in (a) tetragonal (space group $P4mm$), (b) monoclinic (space group Cm) and (c) orthorhombic (space group $Pbam$) phases. Shaded areas indicate the unit cells.

metry, are statistically occupied by Pb ion (this is contrasted to the case where Pb ion is located at 1a site and anisotropic ADPs are used). The structural models used in Rietveld refinements take this into account by assuming that each site is occupied by a quarter of Pb ion. In the case of PZT the four sites are not equivalent, but to a first approximation, the occupation probability of each site does depend on the local B -cation configuration (how the eight nearest B cation sites are occupied). Thus, the Pb-ion displacements are different in the case of Zr- and Ti-rich areas. Cm symmetry allows that spontaneous polarization has a non-zero value in the a -axis direction. In the case of ideal symmetry, this corresponds to coherent Pb-displacements. However, due to the local distortions following spatial composition variation (and changes in bond lengths) also other Pb ion displacements (local disorder) must occur. Thus, there is a delicate interplay between B -cations, oxygen octahedra tilts (if any) and the corresponding Pb-ion displacements. It is not straightforward to say which displacement configuration is energetically the most favourable and is most reliably addressed through experiments. This is demonstrated by PbZrO_3 and PbHfO_3 : due to the large space available for Pb one can construct various hypothetical PbO_4 configurations (different from the experimental ones, such as a one corresponding to a ferroelectric ordering) under the constraint that ions have their nominal valences. It is not obvious when a change to another structure would be favourable. These are aspects to be considered once new materials, such as multiferroics, are designed.

PZT and $\text{Ba}(\text{Zr}_x\text{Ti}_{1-x})\text{O}_3$ (BZT) systems provide interesting case study, since the changes in their electronic band structures versus x are well documented. As was summarized in ref. 43, there are two main differences between Pb perovskites and those containing closed-shell A -cations (such as Ba in the BZT system): (i) the band gap in PZT system is almost constant, being 3.45 eV in PbTiO_3 and 3.72 eV in PbZrO_3 whereas the band gaps in BaTiO_3 and BaZrO_3 are 3.0 and 5.0 eV, respectively and (ii) the presence of shallow Pb^{3+} centers. To understand these observations, band structure computations and electron-paramagnetic-resonance (EPR) spectroscopy studies were carried out for PZT system, reported in refs. 43 and 44 and summarized below. In BZT, the valence band edge consists of O $2p$ states and the conduction band consists of pure Ti/Zr d states⁴⁵. The band gap increases in BZT with x because the Zr $4d$ states lie 2 eV above the Ti $3d$ states and Ba has little effect on the electronic structure because its states lie well away from the band gap. In PZT, the valence band has essentially the same width and character for all x , because this is determined by the Pb s -O p interaction. Similarly to the case of BZT system, the Ti/Zr d states increase rapidly in energy with x . The tight-binding computations for cubic PbTiO_3 and PbZrO_3 revealed that the conduction band minimum is composed of the Ti/Zr d states only at low Zr compositions and switches to Pb $6p$ states with increasing x ^{43,44}. Shallow

Pb^{3+} centers corresponds to a local state slightly above the valence band maximum. EPR experiments revealed that the Pb^{3+} center acquires more Pb $6p$ character with increasing x . This was interpreted to be due to the local off-center displacement of the Pb ion. Thus, by lowering the symmetry of the center the p character is introduced into its wavefunction. The Pb^{3+} hole trap binding energy was found to be between 0.14 and 0.26 eV⁴⁴. These findings were found to be consistent with Raman scattering studies of PZT, Nd-modified PbTiO_3 (PNT) and Nd-modified PZT (PNZT) bulk ceramics using ultraviolet (wavelength 363.79 nm which corresponds to 3.4 eV, close to the band gap energy) and visible light (wavelength 514.532 nm which corresponds to 2.4 eV)⁴⁶. In the case of uv light, several high-frequency modes above 1000 cm^{-1} were observed. Most interestingly, the frequency of the mode at around 1170 cm^{-1} in PZT ceramics showed anomalous behaviour at the well-known phase transitions, corresponding to the changes in Pb ion environment. The use of different systems (PZT, PNT and PNZT) allowed the assignment of these modes to an electronic processes in the Pb^{3+} hole traps⁴⁶, in contrast to Zr and Ti. Once this information is combined with the Pb ion displacements observed through NPD studies one gains very consistent picture of these systems. Now, these observations are important not only for the understanding factors affecting on switchable polarization in Pb-perovskites, but also provide a physical model explaining the activation energies E_A of conductivity in PZT. Values between 0.15 and 0.18 eV were calculated for the E_A assuming Poole-Frenkel mechanism for the conductivity⁴⁷. In many ways analogous situation appears in Bi-perovskites, such as in $(\text{BiScO}_3)_x(\text{PbTiO}_3)_{1-x}$ (BS-PT) alloys⁴⁸. Namely, the large polarization and piezoelectric responses in BS-PT system were found to be due to the Bi/Pb $6p$ -O $2p$ hybridization⁴⁸.

IV. SPATIAL COMPOSITION VARIATION

The PZT system is frequently assumed to be a binary solid solution of PbTiO_3 and PbZrO_3 *without solubility gaps*, as was summarized in ref. 49. According to ref. 49, once a solid solution is formed at high temperature (typically above 800°C), the chemical composition cannot be changed at low temperatures, but the system can have temperature-induced *diffusionless* structural phase transitions. The validity of this assumption has been questioned in refs. 50 and 51 and it was reported that PZT solutions exhibit a positive enthalpy of mixing that suggests *a tendency towards immiscibility and phase decomposition*. Thus, it was proposed⁵¹ that miscibility gaps replace the MPB and the paraelectric to ferroelectric transition lines of the diffusionless phase diagram given in ref. 1 (which would be valid only if the cooling rate significantly exceeds the diffusion rate of Ti and Zr atoms). The analysis was restricted to temperatures above 420 K ⁵¹, although very similar conclusions should

be valid at lower temperatures. Usually the solubility gap increases with decreasing temperature. In the present case the solubility gap and finite atomic diffusion rate would imply that system minimizes its free energy by segregating into two different phases possessing different compositions and crystal symmetries. Although it is probable that the equilibrium situation is not necessarily reached through standard sample preparation techniques, two-phase co-existence is apparent in the vicinity of the MPB. From the microscopic point of view this means that attention should be paid on how Zr and Ti ions are distributed over the B -cation site. This issue was recently addressed in ref. 8 through Monte Carlo type model where the mean of the distribution of cluster volume was analysed as a function of x . This study revealed that the sum of the mean cluster size of the Zr and Ti clusters is a *minimum* at $x = 0.50$, with the most likely minimum volume in which an equal number of Zr and Ti ions is found being 1 nm^3 (for clarity we point out that correspondingly there were many 1 nm^3 volumes with unequal number of Zr and Ti ions). Correspondingly, it was argued that the increase in coherence length of the nano-domains, proposed as the mechanism for the appearance of the macroscopic monoclinic phase close to $x = 0.50$ in ref. 2, may be a consequence of some ordering of the B -cations. According to the model given in ref. 2, the local structures of the $R3m$ and $P4mm$ phases were considered to be monoclinic and Cm phase was interpreted to correspond to those composition and temperature values for which the local regions had grown sufficiently that diffraction techniques see a distinct Cm phase. For the forthcoming discussion, it is important to notice that the spatial composition variation is larger the smaller the spatial length scale is, as is also apparent from Fig. 13 in ref. 8. Our next goal is to estimate the magnitude of the spatial composition variation in simplest terms and to relate it to the experimental observations on local and average structure.

Thus, we assume that the distribution of Zr and Ti is random. For discussion purposes, we further assume that the spatial composition can be divided into two parts: (i) differences between the average compositions of grains, consisted of domains and (ii) composition variation within a domain. To quantify the meaning of spatial composition variation within a domain we assume that the distribution of Zr and Ti obeys the binomial density function with probabilities $p = x$ and $q = 1 - p$ that the B -cation site is occupied by Zr and Ti ion, respectively (the solubility gap would further enhance the spatial composition variation). In principle, ordering effects can be taken into account by introducing conditional probabilities. We believe that the present approximation provides a microscopic explanation for the two phase co-existence observed in the vicinity of the MPB and is consistent with the idea that Cm phase serves as a transitional phase between rhombohedral and tetragonal phases. To see this, we consider the case of PZT with $x = 0.50$: if we divide a large domain (say, with dimen-

sions of the order of $1 \text{ }\mu\text{m}$) to cubes containing N primitive cells, roughly $2/3$ of the cubes contain $N_{\text{Zr}} = xN$ Zr ions with $Np - \sqrt{Npq} \leq N_{\text{Zr}} \leq Np + \sqrt{Npq}$. If we now take the cube edge to be 10 nm (typical spot sizes used in TEM and ED studies are between 1 and 5 nm), almost $1/3$ of the cubes have $x < 0.49$ or $x > 0.51$ (for large values of N binomial distribution can well be approximated by a Gaussian distribution). Spatial composition variation is the probable origin explaining why some domains are rhombohedral, whereas some are monoclinic. In a transition region (compositions between well established rhombohedral and tetragonal regions) Cm phase serves as a transition bridge. The idea of an inhomogeneous distribution of Zr and Ti ions is also consisted with the TEM and ED observations according to which there is a rather large spatial variation in ED patterns as discussed above. Surface phenomena are sensitive to local distortions. It is the feature of the binomial distribution that the variance is largest at around MPB composition ($p \approx q$) and is zero only for pure PbTiO_3 and PbZrO_3 . This is seen from the line widths which increases with increasing x when $0 \leq x \leq 0.50$. This is supported by an atomic pair distribution function analysis carried out for PZT powders with $x = 0.40, 0.52$ and 0.60 ⁵²: the MPB is a crossover point with maximum disorder. It is also important to note that even if the average composition of different grains would be exactly the same, the spatial variation can correspond to domains with different symmetries. In practice, some composition variation in average compositions of different domains and grains exists, as the above mentioned solubility gap suggests. Also the composition of grain boundaries is expectably different from the inner parts. The most important factor behind the two-phase 'co-existences' is probably related to the differences in average compositions of different domains: the domains with larger Zr content can entirely transform to rhombohedral phase, while it looks that the phase transformation cannot be completed in those domains containing larger amount of Ti but is frozen to Cm phase. We note that Cm phase was interpreted to relieve the stress which otherwise would be generated due to the *interacting* rhombohedral and tetragonal domains in ref. 53. From this point of view it is not a surprise that the Bragg reflections of the Cm phase are much wider than those of the $R3c$ phase, and are dependent on temperature. It is our opinion that PZT with composition in the vicinity of the MPB (and similar systems) should be modelled as a two-phase system.

On the other hand, if one could prepare an ideally ordered PZT sample with $x = 0.50$, Cm phase might not be stable. To see this, we note that in the case of ordered PZT with $x = 0.50$ the Zr/Ti distribution is homogeneous in the primitive cell scale and any deviation from this order results in less homogeneous distribution. Correspondingly, there are no Zr rich or deficient areas and in this sense also the mechanism favouring Cm would be missing: if there are no local distortions due to the spatial composition variation, there likely are no domains with

different symmetries (at least not so abundant as the experiments reveal), which in turn implies that there is no need for a phase serving as a bridge between rhombohedral and tetragonal phases. This might be important for a very small grain size powders where most of the grains would be consisted of one domain. Experimentally the two extrema cases, perfect disorder and order, can easily be distinguished by x-ray or neutron diffraction techniques. As the studies dedicated to double perovskites show, ordering is clearly seen from the superlattice reflections in x-ray (for instance, see ref. 54 where polymerized complex method was used to prepare Ba_2MnWO_6 double perovskites) and neutron powder diffraction patterns (see, e.g., ref. 55). Also Raman spectra are consisted with the observed diffraction patterns^{56,57}. As the numerous studies show the difference in ionic radii (and, to a lesser extent, charge) does not provide sufficient driving force for a formation of the double perovskite structure. As proposed in ref. 8, partial ordering may occur, although it is not easy to determine the degree of ordering in the present case. Even though it may not be possible to prepare double perovskite PZT samples the problem can be approached by computational techniques. Finite temperature Monte Carlo simulations carried out for PZT with a broad range of x and random distribution of Zr and Ti in the B -cation site yielded a phase transition sequence $P4mm \rightarrow Cm \rightarrow R3m$ ⁵⁸ (no interaction between different domains was incorporated in this study). Virtual crystal approximation (VCA, where Zr and Ti ions are replaced by the same fictitious average atom) does not reveal a Cm phase⁵⁸. It is an open question if VCA could reproduce Cm phase when the interaction between domains is taken into account. After all, Cm phase always co-exists with rhombohedral phase. The two-phase co-existence in the vicinity of the MPB has proven to be very puzzling and sometimes one can find reports according to which an 'ideal' sample preparation route could yield single phase samples. Recently, an equilibrium phase diagram satisfying the Gibbs phase rule was given in ref. 51. The essential result was that, by the Gibbs phase rule, the single-phase fields on the phase diagram must be separated by two-phase regions (and Cm phase is by no means an exception)⁵¹. According to ref. 17, the flat energy surface near the rhombohedral phase may be the most important factor for high piezoelectric constant materials. As the co-existence suggests, this seems to be the case in PZT system.

V. ANISOTROPIC LINE BROADENING.

The anisotropic (hkl -dependent) line broadening was ascribed to a 'microstrain' in ref. 24. There are several factors which together are responsible for the anisotropic line broadening: (i) Zr substitution for Ti creates local strains due to the size difference, (ii) spatial composition variation: Zr-rich clusters take larger volume per formula unit than Ti-rich clusters, and (iii) Pb-ion shifts

depend on the B -cation environment (i.e., Pb-shifts vary spatially as a response to the spatial variation of the B -cations). Although the given mechanisms are interwoven, the given division serves as a way to estimate which one is dominating at different composition regimes. Thus, the changes in Bragg reflection intensities and displacement parameters in the case of small Zr/Ti substitutions in $\text{PbTiO}_3/\text{PbZrO}_3$ can largely be understood by considering the mechanism (i). Thus, following the treatment given in ref. 59, small Zr substitution for Ti in PbTiO_3 might be treated by considering the concentration of Zr atoms x , the difference between matrix (Ti) and solute (Zr) atoms ΔR . Now, the degree of distortion is characterized by the mean square atomic displacement $\langle U^2 \rangle = jx(\Delta R^2)$, where j is a constant. Static atomic displacements cause a reduction in diffraction peak intensity and increase in diffuse scattering and can be treated in the same way as thermal vibrations. However, this treatment is no more adequate for intermediate values of x since there is no way of selecting such a matrix that experimentally observed features could be explained. Although the mechanism (i) can explain changes in intensities (matrix and solute atoms have different scattering lengths and cross sections) and diffuse scattering (seen as an increased intensity in the Bragg reflection tail regions: the peak width at half maximum is practically not affected by this mechanism) for small values of x , it does not provide a model for changes in Bragg reflection widths. This is why the phenomenological model given in ref. 14 was adopted: it also takes into account the hkl -dependent Bragg reflections widths by introducing a microstrain broadening $\Gamma_S^2 = \sum_{HKL} S_{HKL} h^H k^K l^L$, $H + K + L = 4$. Laue symmetry imposes restrictions on the allowed S_{HKL} terms. Expressions for Γ_S^2 for each Laue symmetry are given in ref. 60.

In addition, we note that rather strong intensity is commonly observed between the $h00$ and $00l$ with $h = l$ Bragg reflections, which was assigned to locally disordered regions in the vicinity of the domains walls in ref. 7. Especially at room temperature it is practically impossible to assign a precise structural model for this phase, since it is not well crystallized. It might also be a precursor phase which at higher Zr contents evolves into a rhombohedral phase. This interpretation was given to the data collected on PHT powders, see Fig. 4 in ref. 26. Nevertheless, scattering from this phase adds intensity to certain diffraction peaks, which in practise also contributes to an asymmetric line broadening (as it is not possible to unambiguously separate it: it is the sum from different contributions what one observes in the case of powder diffraction). For example, the larger and smaller d -spacings sides of the pseudo-cubic 200 and 002 reflections, respectively, seem to gain intensity. Particular care is necessary once this phase is modelled and generally one might do better by collecting data on samples with different Zr contents and at different temperatures.

Although a reasonable structure refinements for

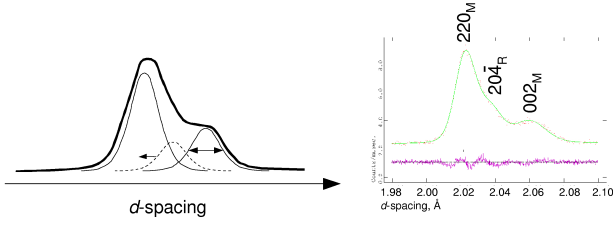


FIG. 3: Left panel: Schematic illustration of the way how the neglect of anisotropic line broadening affects the position of the rhombohedral peaks: once the rightmost peak broadens, it pushes the rhombohedral peak (middle) towards smaller d -spacing. Right panel: Observed and computed high resolution neutron powder diffraction profile collected on PZT with $x = 0.53$ at 4 K. Pseudo-cubic 200 reflection region is shown. Note that the 002_M peak (Cm phase) at around 2.06 \AA is significantly broader than the 220_M (Cm phase) peak at around 2.02 \AA . Now, the position of the rhombohedral 204_R peak depends on the way the line broadening is taken into account. Figure adapted from ref. 61

medium resolution data collected on PZT samples with $x \leq 0.50$ were obtained using a lineshape which ignored anisotropic line broadening, the situation was quite different for high resolution facilities, particularly once the data were collected on two phase samples. In such a case it was essential to use an appropriate profile function. *Now, when the anisotropic line broadening is neglected, the fit in the case of certain weak peaks becomes slightly worse (as was observed to be the case of weak superlattice reflections, which are less weighted in the refinements). The reason for this is illustrated in Fig. 3: in order to improve the fit corresponding to the strong pseudo-cubic 200 reflections, during the refinement the position of $R3c$ reflection is shifted toward higher d -spacings, which in turn resulted in a small shift of the weak peaks at 2.44 and 1.06 \AA . The anisotropic line broadening was not limited to the d -spacing at around 2 \AA , and similar mechanism was seen at other d -spacings. A structural model which reduces the symmetries to 'model' the hkl -dependent line broadening takes local disorder into account incorrectly, since in this way the disorder is assigned to be periodical, obeying the space group symmetry.*

VI. TWO-PHASE MODELS

A. $\text{Pb}(\text{Zr}_{0.52}\text{Ti}_{0.48})\text{O}_3$ and $\text{Pb}(\text{Zr}_{0.53}\text{Ti}_{0.47})\text{O}_3$ samples

In the context of low-temperature phases the role of spatial composition variation was discussed in refs. 5 and 24. The room- and low-temperature crystal symmetry of Zr rich PZT ceramics is $R3c$ ^{4,24,62}, except for the compositions with $x \approx 1$ ⁶³. The room temperature symmetry of PbZrO_3 is $Pbam$ ^{39,64}. Since spatial composition vari-

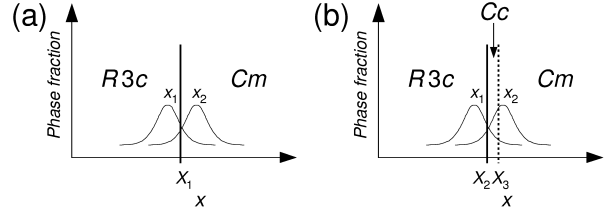


FIG. 4: The consequences of the spatial composition variation (at fixed temperature and pressure) in the case of two samples with average compositions x_1 and x_2 in the vicinity of (a) the phase boundary separating $R3c$ and Cm phases (at X_1) and (b) two phase boundaries separating $R3c$ and Cc (at X_2) and Cc and Cm phases (at X_3). Figure adapted from ref. 61

ation cannot be completely eliminated, there must exist two phases in the vicinity of MPB. Fig. 4 (a) illustrates the consequences of spatial composition variation in the vicinity of MPB at low temperature. To allow the existence of Cc phase necessitates that there should be a narrow region in the $x - T$ plane where this phase is stable or metastable. Now, if we were to explain the existence of Cc phase, two phase boundaries located somewhere between $0.52 \leq x \leq 0.54$ should be assumed to exist, see Fig. 4 (b). This in turn, once the spatial composition variation is taken into account, leads to three phase 'co-existence'. The simplest $Cm + R3c$ model (corresponding to Fig. 4 (a)) was preferred in refs. 5 and 24, since it was able to explain the experimental observations in simplest terms. At low temperature (4 K^{24} or 10 K^{5}) the phase fraction of the Cm phase was monotonically decreasing with x increasing from 0.52 to 0.54 , which in turn implies that two-phase 'co-existence' is predominantly due to the spatial composition variation⁶⁵.

It is worth to point out that the model proposed in ref. 18 was ruled out also in a recent paper, see the last paragraph in ref. 66. After all, the only difference between $Cm + R3c$ model and $Cm + Cc$ model proposed in ref. 66 is that $R3c$ symmetry was used (corresponding to two lattice parameters and four atomic coordinates) instead of the Cc symmetry (corresponding to four lattice parameters and twelve atomic coordinates, although constraints were used to decrease refinable parameters in ref. 66). Now, Cc is a subgroup of $R3c$ space group. Since no superlattice reflections characteristic only to Cc phase were observed (such should appear at large d -spacing region, if symmetry is lowered from $R3c$ to Cc), $R3c$ symmetry was favoured in ref. 5. This allowed considerably simpler structural model: one is tempted to ask how much can be gained by first decreasing the symmetry from $R3c$ to Cc and then decreasing the number of refinable parameters by introducing constraints. This issue is discussed on a more general ground in ref. 67. In ref. 66 the use of Cc phase was largely based on the TEM and ED observations⁶⁸ according to which superlattice

reflections, which were inconsistent with $R3c$ symmetry, were observed at low temperature. This observation is consistent with the observations reported in ref. 32 but the interpretation is entirely different. Now, it would be interesting to consider: (i) similar possibilities as were given in ref. 32 (summarized above), and (ii) if the observed features are only characteristic to TEM samples (layers with thickness between 5 and 100 nm were studied and it was further stated that the size distribution of Cc phase ranged between 3 to 10 nm⁶⁸. This is contrasted by the observation according to which the line widths of $R3c$ phase were much narrower than those of Cm phase²⁴. Neither of the phases was in a form of 'nanoparticles'. It would also be interesting to see how large octahedral tilts are necessary to 'reproduce' the ED patterns, including those superlattice reflections which were taken as an evidence for Cc symmetry, since they were not observed by NPD studies. It is an often overlooked issue that $Cc + Cm$ and $Cm + Cc$ models, given in refs. 18 and 66 respectively, are *completely different* (and mutually exclusive): they present models where Cm and Cc symmetries were swapped. Although this swapping might not be so obvious from studies solely based on TEM/ED techniques it is clearly seen from X-ray powder diffraction and NPD models. In the case of TEM/ED techniques very small volumes are studied in a time (this can also give wrong idea about the phase purity, i.e., if the sample with macroscopic dimensions contains one or two phases) and often no attempts to determine sufficiently accurate lattice parameter were done. Whatever is the reason for overlooking this issue, this type of space group swapping results in entirely different structural parameters and phase fractions. Needless to say, this has nothing to do with composition variation or differences in crystallite sizes, see also related discussion in ref. 69. Despite the increased number of refined parameters, the residuals were still rather high and the differences between different models compared in ref. 18 were marginal. For instance, R_{exp} was lowest for the $Cm + R3c$ model which was rejected in ref. 18. As discussed in the next section, the model given in ref. 18 does not assign octahedral tilts to a correct phase. In contrast, the models proposed in refs. 5 and 66 assigned octahedral tilts to the same phase. In the case of the data shown in ref. 18 the intensity of the peak(s) at around 1.06 Å was barely above the noise level and the $Cc + Cm$ model assigns more reflections than there are data points in this region. Thus these reflections do not provide justification for the use of Cc phase.

In addition, some reports claimed that dielectric measurements gave support to Cc phase (for example, see ref. 20). Although these types of measurements might be useful once phase transitions in single phase samples are studied, not too much emphasis should be put on data collected on multiphase samples. In this context we note that the samples studied in refs. 70 and 71 contained a nonidentified impurity phase(s), as was revealed by the peaks at around 28 and 35 two-theta degrees (corre-

sponding to d spacings 3.18 Å and 2.56 Å, respectively), in addition to the aforementioned two-phase co-existence. This implies that the composition was not well known and thus the possibility of compositional and structural inhomogeneities should be kept in mind. Although this non-perovskite phase was well resolved, it was not included in the Rietveld refinement model considered in ref. 70, which in turn results in an error in the structural parameters of the perovskite phase(s). This is likely related to the fact that the diffraction pattern shown in ref. 70 (reported to have $x = 0.52$) is reminiscent to the diffraction pattern with $x = 0.53$ shown in ref. 5. In contrast, the diffraction pattern with $x = 0.52$ given in ref. 16) and the diffraction pattern of the $x = 0.52$ sample reported in refs. 66 and 6,7 were reminiscent.

B. $\text{Pb}(\text{Zr}_{0.54}\text{Ti}_{0.46})\text{O}_3$ sample

The anisotropic line broadening and the absence of the superlattice reflection evidencing Cc symmetry in PZT powders with $x = 0.52$ and $x = 0.53$ provided a motivation to carry out a subsequent study using a high resolution NPD instrument²⁴. To model the peak profiles, GSAS⁶⁰ lineshape 4 by Stephens¹⁴ was used in this study. In addition, Zr content was slightly increased to $x = 0.54$ ²⁴ (although it was possible to fit *all* reflections using the $Cm + R3c$ model also in the case of $x = 0.52$ and $x = 0.53$ samples). This allowed a more reliable refinement and symmetry identification to be done by studying the *changes in phase fractions versus temperature*. Importantly, for these compositions it has been found that oxygen octahedra tilts increase with increasing x (see ref. 4) and decreasing temperature (this feature is discussed in refs. 3 and 5). We also note that previously Cc was proposed to be a space group symmetry corresponding to high isotropic pressure³⁷, whereas the present review concentrates on the determination of space group symmetries versus composition and temperature at ambient pressure. Now, PZT sample with $x = 0.54$ provided a test for clarifying which phase is the preferred one at low temperature. This is of particular interest also from the point of view of *ab initio* computations dedicated for PZT according to which the largest piezoelectric d_{33} coefficients are found to be large namely in the rhombohedral side of the MPB: much smaller values were found in the tetragonal side of the MPB⁷². These observations are consistent with the experimental observations on PZT⁷³ and $\text{Pb}(\text{Zn}_{1/3}\text{Nb}_{2/3})\text{O}_3\text{-PbTiO}_3$ (PZN-PT) and $\text{Pb}(\text{Mg}_{1/3}\text{Nb}_{2/3})\text{O}_3\text{-PbTiO}_3$ (PMN-PT)⁷⁴ (the two latter systems also possess MPB separating rhombohedral and tetragonal phases). The NPD data in ref. 24 suggests the following phase transition sequence with decreasing temperature in the vicinity of MPB: $Pm\bar{3}m \rightarrow P4mm \rightarrow Cm \rightarrow R3m \rightarrow R3c$ where adjacent groups have a group-subgroup relationship. Due to the composition variation some domains undergo the same phase transition sequence at higher (Zr richer) or lower

(Ti richer) temperatures. This sequence demonstrates the role of Cm phase linking $P4mm$ and $R3m$ phases. The co-existence of the rhombohedral and Cm phase is consistent with the idea that they are energetically almost as favourable and rather small changes in temperature, pressure or an applied electric field can transform Cm phase to rhombohedral phase. First-principles computational study revealed that the electric field induced phase transformation sequence with an increasing applied electric field was found to be reversed when the field was released⁷², whereas the same was not found experimentally in ref. 75. This different behaviour was attributed to defects⁵⁸: the model used in *ab initio* computations was defect free, whereas in practice they cannot be completely eliminated. In this context it is interesting to note the domain switching in $Pb(Zr_{0.49}Ti_{0.51})O_3$ sample, where tetragonal and rhombohedral (volumetric phase fractions 79 and 21 %, respectively) phases were present, studied through in situ uniaxial compression experiments⁷⁶. Data were analysed via Rietveld refinement which allowed texture and lattice strains to be simultaneously determined. It was found that the rhombohedral phase responds more readily both to electric fields and applied stress.

As is seen from Fig. 1 in ref. 24, once the crystals are compressed with decreasing temperature, the $R3c$ phase was favoured and Cm phase did not transform to Cc phase, in strong contrast with the model proposed in ref. 18). We note that the volume of the $R3c$ phase grows with decreasing temperature (for instance, see Fig. 1 in ref. 24). Thus, no evidence was found for the $P4mm \rightarrow Cm \rightarrow Cc$ phase transition sequence. When the oxygen octahedra had almost no chance to contract, they were rotated to opposite directions along the pseudo-cubic 111 axis (tilt system $a^-a^-a^-$). This tilt results in a decrease of the volume of cuboctahedra around Pb ions. Changes evidencing Cc symmetry (and the corresponding tilt system) were not observed. *Indeed, the phase fraction of Cm phase (which was assigned to Cc symmetry in ref. 18) decreased with decreasing temperature, whereas $R3c$ phase fraction significantly increased with decreasing temperature.* This can be confirmed by a naked eye observation of the diffraction patterns in Fig. 1 in ref. 24, although the results of refinements were also given. The intensity of the peak at around 1.06 Å was increasing with decreasing temperature, which further confirmed that its origin is the phase assigned to $R3c$ phase. Also the peak at around 1.06 Å was well fit by $R3c$ symmetry. In other words, in ref. 18 Cc phase was used to model the Bragg reflection from the pseudo-tetragonal phase and also the superlattice reflections. Thus, Cc symmetry was used to model Bragg peak from two distinct phases, which is not correct. However, the temperature and composition dependence clearly show that when the phase fraction of Cm phase decreased, the intensity of the superlattice reflection was increasing together with the phase fraction of $R3c$ phase. This behaviour is consistent with the composition vari-

ation: the distortion (monoclinic or rhombohedral) and the volume of the distortion depend on average composition and temperature.

VII. CORRELATION BETWEEN THE c/a AXIS RATIO AND PIEZOELECTRIC CONSTANTS

It is of interest to compare the recent computational results with the structural parameters obtained through structural studies. According to the computations carried out for $PbTiO_3$ and $Pb(Zr_{0.50}Ti_{0.50})O_3$ (where Zr and Ti atoms were alternatively occupying the B -cation layers perpendicular to the c axis) the fixed volume piezoelectric constants $e_{33,v} = e_{33} - 0.5(e_{31} + e_{32})$ and $e_{13,v} = e_{13} - 0.5(e_{11} + e_{12})$ become very large in the range $1.0 < c/a < 1.02$ ⁷⁷. Experiments have shown that the c axis remains almost constant for $0 < x < 0.50$, whereas a axis increases almost linearly for these compositions, corresponding to a steady decrease of the c/a axis ratio⁵. However, in the MPB region the c/a axis ratio decreases dramatically: averaging monoclinic a and b axes the c/a is found to be 1.01 for $x = 0.54$ ²⁴. Fig. 5 shows the room temperature c/a axis ratios. It is seen that the ratio strongly decreases once x increases from 0.50 to 0.54. This is consistent with the idea that Cm phase continuously transforms to rhombohedral phase. For pure $PbTiO_3$ *ab initio* computations show that $P4mm$ phase is energetically more favourable than the $R3m$ phase, consistently with the experimental observation. This means that the electric field, which in practice can be applied (without electric breakdown), does not induce a phase transition sequence $P4mm \rightarrow Cm \rightarrow R3m$ and, via the polarization rotation model, piezoresponse remains much lower than in the case of PZT in the vicinity of the MPB. However, recent computational study demonstrated that pressure can induce a MPB in $PbTiO_3$ ⁷⁹. It was found that pressure induced a phase transition sequence $P4mm \rightarrow Cm \rightarrow R3m \rightarrow Pm\bar{3}m$, together with large piezoelectric coupling coefficients in the transition regions⁷⁹.

VIII. BOND-VALENCE SUMS AND ION VALENCES

Computations of bond valence sums (BVS) provides a way to test whether the bond lengths are reasonable. Although it is not sensitive for minor changes in symmetry, unless bond lengths are altered, it has proven to be useful for confirming the effect of the proposed Pb, Zr and Ti ion displacements⁵. Namely, if Pb ions are constrained to be located in their ideal positions in the case of $P4mm$ phase, the Pb ion valence would be $\approx +1.8$, whereas it is quite close to the nominal valence +2 once Pb ions are allowed to be displaced towards $\langle 110 \rangle$ directions. This is actually rather general tendency for Pb ion and occurs in rhombohedral phases. This is quite plausible since the

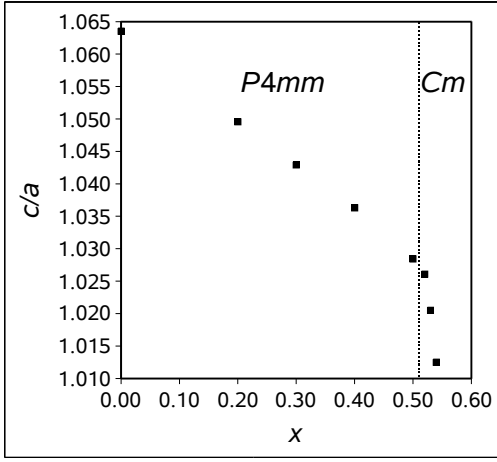


FIG. 5: Experimentally determined room temperature c/a axis values for PZT ceramics. Lattice parameters were adapted from ref. 78 (PbTiO_3) and refs. 5 and 24 (PZT).

cuboctahedra is so large that if Pb ion would occupy its centre, it would result in valence deficient Pb ions. Thus, by forming four short bonds with oxygen more reasonable valence values for Pb are achieved. Similarly, the average B -cation valence $v(B_{av}) = xv(\text{Zr}) + (1-x)v(\text{Ti})$ was +4 when Zr and Ti ions were allowed to have different fractional coordinates. In the case of the tetragonal PZT it was demonstrated that if one insists to constrain the fractional coordinates to be the same, no Wyckoff $1b$ position in the unit cell would correspond to the nominal valence +4. It also worth to point out that if Pb ions are constrained to be at the $1a$ site symmetry position Pb ADPs are very large. On the other hand, by constraining the B cations to have the same fractional coordinates yielded negative ADP values. Allowing Pb ions to be displaced towards $\langle 110 \rangle$ directions and Zr and Ti ions to have different fractional z -coordinates resulted in physically reasonable ADP values. From this point of view it was important to check the validity of the structural models by confirming that both anomalous valence and ADP values can be eliminated by the same structural model. Oxygen valences in PZT systems were close to their nominal valence value -2 . Also oxygen ADP values were reasonable. Thus, as far as NPD studies are considered, it is a decent approximation to assume oxygen octahedra to fulfil the requirements of space group symmetry, in contrast to the case of cation positions. This also implied that it was not necessary to invoke the plausible mechanism, the expansion of Zr octahedra and contraction of Ti octahedra, to correct the anomalously large Zr and small Ti valences in the structural models used to model the NPD data.

BVS were found to be consistent with the observed phase transition sequences so that reasonable valence values for each ion were obtained also in the case of the Cm and $R3c$ phases. The relationship between the oxygen octahedra and cuboctahedra volumes and octahedra tilts

were pointed out in ref. 3. Namely, $R3c$ symmetry allows oxygen octahedra tilt, which means that the volume of oxygen octahedra increases with increasing tilt angle. This in turn allows the valence of each ion to be close to their nominal values. The same is not possible in the case of $R3m$ symmetry and thus the observed oxygen octahedra tilts versus temperature and x seen in the case of PZT samples with $x = 0.52$ and $x = 0.53$ are consistent with the 'constraints' set by nominal valences⁵. In many ways similar findings, based on density functional theory computations carried on PZT modelled with large supercells, were reported in ref. 80. Perhaps the most essential difference between the typical Rietveld refinement models and supercell models for PZTs is that the space group symmetries used in the latter approach allow different size oxygen octahedra for Zr and Ti, whereas they are constrained to be the same in Rietveld refinements (one actually replaces both Zr and Ti by a 'pseudo-atom' whose scattering length (NPD) or cross section (X-ray diffraction) is a weighted average over Zr and Ti ions). This explains why the individual bond-valences for Zr and Ti were found to be close to their nominal values in the case of the supercell computations⁸⁰. In this sense it is surprising to see that both approaches support the idea that oxygen position do not suffer from local distortions to the extent cation positions do.

IX. CONCLUSIONS

The pitfalls related to the modelling of the crystal structures of PZT ceramics with different compositions and at different temperatures were reviewed. The role of the spatial composition variation, resulting in two-phase 'co-existence' in the vicinity of the phase boundaries and anisotropic line broadening, were reviewed. The conditions set to sample preparation, powder diffraction instrument and line shape were addressed. Focus was put on the structure analyses on PZT ceramics with compositions in the vicinity of the morphotropic phase boundary (MPB). Recent studies pointed out that the two-phase co-existence in the vicinity of the phase boundary is a thermodynamical necessity in PZT system and further is very crucial for the high electromechanical coupling coefficients observed in MPB compositions. Two different approaches for modelling the two-phase structures of PZT ceramics with compositions corresponding to the MPB were identified. The first is a method where space group symmetry was decreased so that both local and average crystal symmetries were modelled, whereas the second method was based on the highest space group symmetry compatible with the observed Bragg reflections and where local distortions were taken into account by selecting an appropriate line shape. Recently published $Cm + Cc$ and $Cc + Cm$ structure models were compared with $Cm + R3c$ model where anisotropic line shapes were used. Whereas $Cm + R3c$ model is a higher symmetry version of $Cm + Cc$ model, $Cc + Cm$ model was shown

to be inapplicable. Once the local distortions, resulting in anisotropic line broadening, are correctly taken into account, we do not find support for $Cm + Cc$ model. Instead we found that $Cm + R3c$ model describes all Bragg peaks and their intensities well. It was further shown that the $Cm + R3c$ model is consistent with the structural features observed at other compositions and temperatures, which is particularly important in the vicinity of the phase boundary. Also issues related to the effects of a finite sample size used in transmission electron microscopy and electron diffraction (ED) studies were discussed and it was pointed out that while locally ordered areas may occur in nanosize samples, resulting in additional reflections in ED patterns, they frequently do not appear in bulk samples. Thus, the same structural model might not be valid for nanoscale and bulk samples. It was

further pointed out that these features are not limited to MPB compositions. Spatial variation of Pb ions shifts follows from the spatial variation in the B -cation distribution. This is believed to be important for explaining the experimental structural data and for understanding electrical conductivity and piezoelectric properties. Connection between the structural parameters and piezoelectric properties were discussed in light of the recent computational studies.

Acknowledgments

Author is grateful for the Academy of Finland for financial support (Project numbers 207071 and 207501).

-
- * Electronic address: jfr@fyslab.hut.fi
- ¹ B. Jaffe, W. R. Cook and H. Jaffe, *Piezoelectric Ceramics*, (Academic Press, London, 1971).
 - ² A. M. Glazer, P. A. Thomas, K. Z. Baba-Kishi, G. K. H. Pang and C. W. Tai, *Phys. Rev. B* **70**, 184123 (2004).
 - ³ N. W. Thomas and A. Beitollahi, *Acta Cryst. B* **50**, 549 (1994).
 - ⁴ D. L. Corker, A. M. Glazer, R. W. Whatmore, A. Stallard, and F. Fauth, *J. Phys. Condens. Matter* **10**, 6251 (1998).
 - ⁵ J. Frantti, S. Ivanov, S. Eriksson, H. Rundlöf, V. Lantto, J. Lappalainen, and M. Kakihana, *Phys. Rev. B* **66**, 064108 (2002).
 - ⁶ B. Noheda, D. E. Cox, G. Shirane, J. A. Gonzalo, L. E. Cross and S-E. Park, *Appl. Phys. Lett.* **74**, 2059 (1999).
 - ⁷ B. Noheda, J. A. Gonzalo, L. E. Cross, R. Guo, S-E. Park, D. E. Cox, and G. Shirane, *Phys. Rev. B* **61**, 8687 (2000).
 - ⁸ A. J. Bell, *J. Mater. Science* **41**, 13 (2006).
 - ⁹ W. F. Kuhs, in *International Tables for Crystallography. Volume D: Physical Properties of Crystals*, Ed. A. Authier, (Kluwer Academic Publishers, Dordrecht/Boston/London 2003), p. 228.
 - ¹⁰ C. M. Foster, Z. Li, M. Grimsditch, S. K. Chan, and D. J. Lam, *Phys. Rev. B* **48**, 10160 (1993).
 - ¹¹ J. Frantti and V. Lantto, *Phys. Rev. B* **54**, 12139 (1996).
 - ¹² J. Frantti and V. Lantto, *Phys. Rev. B* **56**, 221 (1997)
 - ¹³ N. A. Hill, *J. Phys. Chem. B* **104**, 6694 (2000).
 - ¹⁴ P. W. Stephens, *J. Appl. Crystallogr.* **32** 281 (1999).
 - ¹⁵ A. Leineweber and E. J. Mittemeijer, *J. Appl. Cryst.* **37** 123 (2004).
 - ¹⁶ J. Frantti, J. Lappalainen, S. Eriksson, V. Lantto, S. Nishio, M. Kakihana, S. Ivanov, and H. Rundlöf, *Jpn. J. Appl. Phys.* **39**, 5697 (2000).
 - ¹⁷ H. Fu and R. E. Cohen, *Nature* **403**, 281 (2000).
 - ¹⁸ R. Ranjan, A. K. Singh, Ragini, and D. Pandey, *Phys. Rev. B* **71**, 092101 (2005).
 - ¹⁹ For clarity we note that this report was based on previously published neutron powder diffraction data. Same powder diffraction pattern was given in refs. 20 and 21, where it was modelled by Pc and Cc symmetries, respectively. Thus, they were both single phase models, which actually seems to be the origin of the problems in their structural models: reflections corresponding to two phases were modelled by a single low-symmetry phase.
 - ²⁰ R. Ranjan, S. K. Mishra, D. Pandey and K. Kennedy, *Phys. Rev. B* **65**, 060102 (2002).
 - ²¹ D. M. Hatch, H. T. Stokes, R. Ranjan, Ragini, S. K. Mishra, D. Pandey, and B. J. Kennedy, *Phys. Rev. B* **65**, 212101 (2002).
 - ²² In this paper we use both terms 'locally ordered regions' and 'local distortions' to emphasize the difference between ordered regions possessing short range order in cations shifts in a scale of a few unit cells and deviations from the average symmetry lacking any short range order. An example of the former is given in refs. 2 and 4, whereas inhomogeneous distributions of different size B -cations result in spatial variation of the lattice parameters.
 - ²³ One can make the difference between measured and calculated diffraction intensities arbitrarily small by simply using space group $P1$ and increasing the primitive cell size until the difference is below the desired value.
 - ²⁴ J. Frantti, S. Eriksson, S. Hull, V. Lantto, H. Rundlöf, and M. Kakihana, *J. Phys.: Condens. Matter* **15**, 6031 (2003).
 - ²⁵ Y. Ikeuchi, S. Kojima and T. Yamamoto, *Jpn. J. Appl. Phys.* **36**, 2985 (1997).
 - ²⁶ J. Frantti, Y. Fujioka, S. Eriksson, S. Hull and M. Kakihana, *Inorg. Chem.* **44**, 9267 (2005).
 - ²⁷ J. Frantti, V. Lantto, S. Nishio and M. Kakihana, *Phys. Rev. B* **59**, 12 (1999).
 - ²⁸ J. Frantti, J. Lappalainen, S. Eriksson, V. Lantto, S. Nishio, M. Kakihana, S. Ivanov, and H. Rundlöf, *Jpn. J. Appl. Phys.* **38**, 5679 (1999).
 - ²⁹ J. Frantti, Y. Fujioka, S. Eriksson, V. Lantto, and M. Kakihana, *Journal of Electroceramics* **13**, 299 (2004).
 - ³⁰ G. A. Rossetti, Jr., P. F. Cahill, Jr., R. R. Biederman and A. Sacco, Jr., *Mater. Lett.* **41**, 72 (1999).
 - ³¹ D. Viehland, *Phys. Rev. B* **52**, 778 (1995).
 - ³² J. Ricote, D. L. Corker, R. W. Whatmore, S. A. Impey, A. M. Glazer, J. Dec and K. Roleder, *J. Phys. Condens. Matter* **10**, 1767 (1998).
 - ³³ A. M. Glazer, *Acta Cryst. A* **31** 756 (1975).
 - ³⁴ K. Leung, *Phys. Rev. B* **67**, 104108 (2003).
 - ³⁵ M. Born and K. Huang, *Dynamical Theory of Crystal Lattices*, Oxford University Press, 1988.
 - ³⁶ R. A. Cowley, *Acta Cryst.* **15**, 687 (1962).

- ³⁷ J. Rouquette, J. Haines, V. Bornand, M. Pintard, Ph. Papat, W. G. Marshall, and S. Hull, *Phys. Rev. B* **71**, 024112 (2005).
- ³⁸ D. Le Bellac, J. M. Kiat, P. Garnier, H. Moudden, Ph. Sciau, P. A. Buffat and G. André, *Phys. Rev. B* **52**, 13184 (1995).
- ³⁹ D. L. Corker, A. M. Glazer, J. Dec, K. Roleder and R. W. Whatmore, *Acta Cryst. B* **53** 135 (1997).
- ⁴⁰ D. L. Corker, A. M. Glazer, W. Kaminsky, R. W. Whatmore, J. Dec and K. Roleder, *Acta Cryst. B* **54** 18 (1998).
- ⁴¹ R. W. Whatmore and A. M. Glazer, *J. Phys. C: Solid State Phys.* **12**, 1505 (1979).
- ⁴² S. Teslic and T. Egami, *Acta Cryst. B* **54** 750 (1998).
- ⁴³ W. L. Warren, J. Robertson, D. Dimos, B. A. Tuttle, G. E. Pike and D. A. Payne, *Phys. Rev. B* **53**, 3080 (1996).
- ⁴⁴ J. Robertson, W. L. Warren and B. A. Tuttle, *J. Appl. Phys.* **77**, 3975 (1995).
- ⁴⁵ R. D. King-Smith and D. Vanderbilt, *Phys. Rev. B* **49**, 5828 (1994).
- ⁴⁶ J. Frantti, V. Lantto and M. Kakihana, *Jpn. J. Appl. Phys.* **37**, 5406 (1998).
- ⁴⁷ J. Lappalainen, J. Frantti and V. Lantto, *J. Appl. Phys.* **82**, 3469 (1997).
- ⁴⁸ J. Íñiguez, D. Vanderbilt and L. Bellaiche, *Phys. Rev. B* **67**, 224107 (2003).
- ⁴⁹ W. Cao and L. E. Cross, *Phys. Rev. B* **47**, 4825 (1993).
- ⁵⁰ M. V. Rane, A. Navrotsky and G. A. Rossetti, Jr, *J. Solid State Chem.* **161**, 402 (2001).
- ⁵¹ G. A. Rossetti, Jr., W. Zhang and A. G. Khachatryan, *Appl. Phys. Lett.* **88**, 072912 (2006).
- ⁵² W. Dmowski, T. Egami, L. Faber and P. K. Davies, in *Fundamental Physics of Ferroelectrics-Eleventh Williamsburg Ferroelectric Workshop*, edited by R. E. Cohen (American Institute of Physics, Melville, NY, 2001), p. 33.
- ⁵³ V. Topolev and A. Turik, *J. Phys.: Condens. Matter* **13**, 771 (2001).
- ⁵⁴ Y. Fujioka and M. Kakihana, *Trans. Mater. Res. Jpn.* **28**, 373 (2003).
- ⁵⁵ A. K. Azad, S. Ivanov, S.-G. Eriksson, J. Eriksen, H. Rundlöf, R. Mathieu and P. Svedlindh, *Mater. Res. Bull.* **36**, 2215 (2001).
- ⁵⁶ Y. Fujioka, J. Frantti and M. Kakihana, *J. Phys. Chem.* **110**, 777 (2005).
- ⁵⁷ M. Liegeois-Duychaerts P. Tarte, *Spectrochim. Acta* **30A**, 1711 (1974).
- ⁵⁸ L. Bellaiche, A. García, *Phys. Rev. Lett.* **84**, 5427 (2000).
- ⁵⁹ L. S. Zevin and G. Kimmel, *Quantitative X-ray Diffractionmetry* (Springer-Verlag, New York, 1995), p. 263.
- ⁶⁰ A. C. Larson and R. B. Von Dreele, *General Structure Analysis System*, LANSCE MS-H805, Los Alamos National Laboratory, Los Alamos, NM 87545 (2000).
- ⁶¹ J. Frantti. (2005-07-04) oai:arXiv.org:cond-mat/0504432.
- ⁶² C. Michel, J. M. Moreau, G. D. Achenbach, R. Gerson, and W. J. James, *Solid State Commun.* **7**, 865 (1969).
- ⁶³ The situation might be different for a high pressure case or at low temperatures in the case of the Zr rich PZT (e.g., for $x \geq 0.60$) since the octahedral tilting allowed by $R3c$ symmetry might no more be sufficient. If so, one could expect that this phase extends to a larger values of x . One may also speculate if symmetries allowing different octahedral tilts could be stabilized in the case of strained thin films.
- ⁶⁴ A. M. Glazer, K. Roleder and J. Dec, *Acta Cryst. B* **49** 846 (1993).
- ⁶⁵ Although spatial composition variation is mainly responsible for the two-phase co-existence and line broadening phenomena, other factors, such as crystal size, have an effect on line broadening and probably affect phase fraction estimations.
- ⁶⁶ D. E. Cox, B. Noheda, and G. Shirane, *Phys. Rev. B* **71**, 134110 (2005).
- ⁶⁷ W. Massa, *Crystal Structure Determination*, (Springer-Verlag, Berlin, 2000), p. 157.
- ⁶⁸ B. Noheda, L. Wu and Y. Zhu, *Phys. Rev. B* **66**, 060103 (2002).
- ⁶⁹ B. Noheda and D. E. Cox, (2005-11-10) oai:arXiv.org:cond-mat/0511256.
- ⁷⁰ Ragini, R. Ranjan, S. K. Mishra, and D. Pandey, *J. Appl. Phys.* **92**, 3266 (2002).
- ⁷¹ Ragini, S. K. Mishra, D. Pandey, H. Lemmens, and G. Van Tendeloo, *Phys. Rev. B* **64**, 054101 (2001).
- ⁷² L. Bellaiche, A. García, *Phys. Rev. B* **64**, 060103 (2001).
- ⁷³ X. Du, J. Zheng, U. Belegudu and K. Uchino, *Appl. Phys. Lett.* **72**, 2421 (1998).
- ⁷⁴ S.-E. Park and T. Shrout, *J. Appl. Phys.* **82**, 1804 (1997).
- ⁷⁵ B. Noheda, D. E. Cox, G. Shirane, S.-E. Park, L. E. Cross and Z. Zhong, *Phys. Rev. Lett.* **86**, 3891 (2001).
- ⁷⁶ R. C. Rogan, E. Üstündag, B. Clausen, M. R. Daymond, *J. Appl. Phys.* **93**, 4104 (2003).
- ⁷⁷ Z. Wu and H. Krakauer, *Phys. Rev. B* **68**, 014112 (2003).
- ⁷⁸ A. M. Glazer and S. A. Mabud, *Acta Cryst. B* **34** 1065 (1978).
- ⁷⁹ Z. Wu and R. E. Cohen, *Phys. Rev. Lett.* **95**, 037601 (2005).
- ⁸⁰ I. Grinberg, V. R. Cooper and A. M. Rappe, *Phys. Rev. B*, 144118 (2004).